JACS
JOURNAL OF THE AMERICAN CHEMICAL SOCIETY
Communication
pubs.acs.org/JACS

Flexible Three-Dimensional Nanoporous Metal-Based Energy Devices

Yang Yang,[†,‡,⊥] Gedeng Ruan,[†,⊥] Changsheng Xiang,[†] Gunuk Wang,[†,‡] and James M. Tour*[,†,‡,§]

[†]Department of Chemistry, [‡]Smalley Institute for Nanoscale Science and Technology, and [§]Department of Material Science and NanoEngineering, Rice University, 6100 Main Street, Houston, Texas 77005, United States

Supporting Information

ABSTRACT: A flexible three-dimensional (3-D) nanoporous NiF_2-dominant layer on poly(ethylene terephthalate) has been developed. The nanoporous layer itself can be freestanding without adding any supporting carbon materials or conducting polymers. By assembling the nanoporous layer into two-electrode symmetric devices, the inorganic material delivers battery-like thin-film supercapacitive performance with a maximum capacitance of 66 mF cm^{-2} (733 F cm^{-3} or 358 F g^{-1}), energy density of 384 Wh kg^{-1}, and power density of 112 kW kg^{-1}. Flexibility and cyclability tests show that the nanoporous layer maintains its high performance under long-term cycling and different bending conditions. The fabrication of the 3-D nanoporous NiF_2 flexible electrode could be easily scaled.

Advances in soft portable electronic devices (PEDs), such as roll-up touch screen displays, artificial electronic skin, e-paper, and wearable systems for both personal and military uses, require the development of flexible energy devices.[1,2] Flexible supercapacitors or electrochemical capacitors (ECs) can be based on non-faradaic electrostatic adsorption, such as in electric double-layer capacitors (EDLCs) on carbon materials. Or their behavior can be based upon faradaic redox reactions such as in pseudocapacitors made from transition metal oxides. These flexible EC devices are displaying an increasing role in portable energy storage devices due to their fast dynamic responses, long-term cyclability, and integrated advantages over conventional capacitors (for high power) and batteries (for high energy).[3,4] From a practical viewpoint, for use in PEDs, it is necessary to achieve high capacitance within a limited area or volume, since PEDs are small in size.[5] Hence, areal capacitance (C_A) and volumetric capacitance (C_V), rather than the conventionally used gravimetric capacitance,[6] are better indications of the performance. Conducting polymers such as polyaniline and various carbon-based materials, including carbon nanotubes (CNTs), reduced graphene oxide (rGO), and carbon fibers, deliver low C_A and C_V due to their low densities (less than 2 g cm^{-3}), although they have high flexibility.[7,8]

The poor mechanical flexibility of inorganic metal compounds with high C_A and C_V, having the general formula MX (X = O, N, or F), has been improved by forming hybrid composites using conducting polymers or carbon-based materials as the matrix, or by manufacturing the materials into nanostructures.[9−12] Three-dimensional (3-D) nanoporous structures hold promise due to their good flexibility and high surface area. The nanopores lead to enhancement of the performance of the ECs by facilitating ion transport and creating more-active reaction sites.[13,14] Here we present a technique to fabricate 3-D nanoporous NiF_2-dominant flexible thin-film energy storage devices. The fabricated thin-film can be freestanding, without support from other carbon materials and conducting polymers. The technique is scalable for possible mass production and could be extended to fabricate freestanding all-solid-state electrodes. The technique also has the potential to be applied to fabricate other 3-D metal nanoporous materials. NiF_2 was used in this study due to the large operation potential window of metal fluorides and the possibility to convert NiF_2 to $Ni(OH)_2$ under certain electrochemical conditions (see the Supporting Information (SI)), which would produce an extremely high theoretical capacitance of 2082 F g^{-1}.[15]

To fabricate flexible devices based on nanoporous NiF_2-dominant thin-film electrodes for supercapacitor applications, nickel was electrodeposited on Au/Cr/poly(ethylene terephthalate) (PET) substrates (Figure 1a). Anodization was then used to electrochemically etch the deposited nickel to form a 3-D nanoporous structure. The as-prepared 3-D nanoporous layer (NPL) on the substrate showed good flexibility (Figure 1b) due to the enhanced mechanical properties conveyed by the nanoporous structure.[16] The NPL became freestanding after removal of the substrate (Figure 1c). The fabricated thin film with the NPL had a thickness of ∼900 nm and an average pore size ∼5 nm, as confirmed by scanning electron microscopy (SEM) observation from different viewing directions: cross-sectional (Figures 1d and S1a,b), top (Figure 1e), and bottom (Figure 1f). The NPL with an average pore size of ∼5 nm was also observed by transmission electron microscopy (TEM, Figures 1g and S1c,d). The identified *d*-spacing from high-resolution TEM (HRTEM) was ∼0.32 nm, which corresponds to the NiF_2 (110) plane, as indicated by the lattice fringes (Figure 1g).[17] To investigate the porous structure of the NPL, Brunauer−Emmett−Teller (BET) analysis by adsorption/desorption of nitrogen gas was performed. The data were used to determine the Barrett−Joyner−Halenda (BJH) pore size. Nanoscale pores distributed mainly in a range from 2 to 10 nm were observed (Figure S2). Furthermore, X-ray photoelectron spectroscopy (XPS) analysis (Figure S3) also confirms that the as-prepared NPL is mainly composed of Ni and F. The Ni 2p spectrum indicates Ni is mostly bound to F to form NiF_2. The detected O 1s and C 1s spectra are from the adsorbed

Received: February 5, 2014
Published: April 15, 2014

   dx.doi.org/10.1021/ja501247f | *J. Am. Chem. Soc.* 2014, 136, 6187−6190

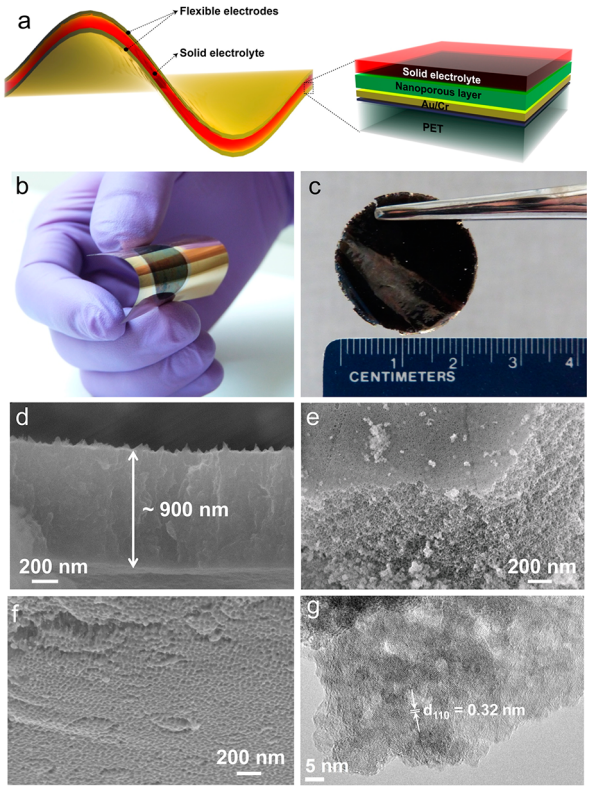

Figure 1. Structure of the 3-D nanoporous layer (NPL) and electrode schematic. (a) Schematic of the flexible NPL on Au (~40 nm)/Cr (~10 nm)/PET substrate (~35 μm). The figure on the right is only half of the final embodiment. Atop the solid electrolyte layer is another nanoporous layer, then Au/Cr, and finally PET to complete the sandwich structure. More specifically, there is one solid electrolyte layer separating two halves of nanoporous layer, Au/Cr, and PET. The entire sandwich shown at left is ~170 μm thick. (b) Photograph of flexible electrode under bending. (c) The freestanding NPL after removal of the substrate. (d–f) SEM images taken from different viewing directions: cross section, top, and bottom, respectively. (g) HRTEM image of the NPL.

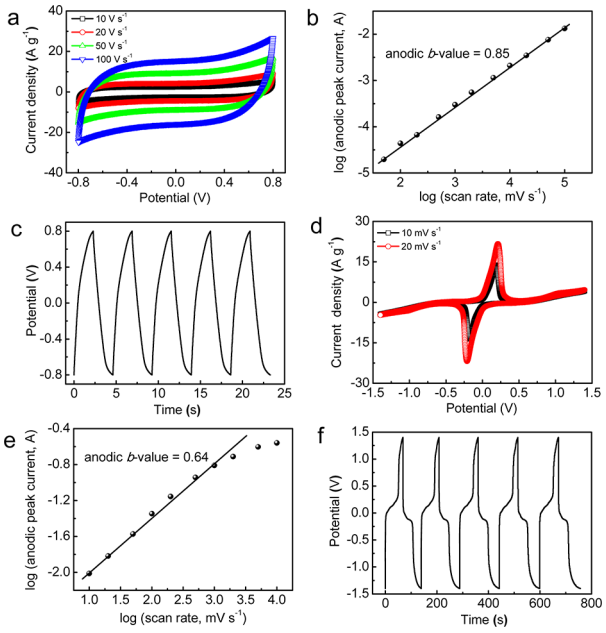

Figure 2. Electrochemical capacitor (EC) performances of the NPL in two-electrode symmetric devices within different potential windows: (a–c) NPW (−0.8 to 0.8 V) and (d–f) WPW (−1.4 to 1.4 V). (a) CVs of the NPL at different scan rates from 10 to 100 V s^{-1}. (b) Log(anodic peak current) vs log(scan rate) plot. (c) Galvanostatic discharge/charge (GDC) curves of the NPL at a current density of 0.1 mA cm^{-2}. (d) CVs of the NPL at 10 (black line) and 20 (red line) mV s^{-1}. (e) Log(anodic peak current) vs log(scan rate) plot. (f) GDC curves of the NPL at current density of 1 mA cm^{-2}.

moisture and CO_2 from the atmosphere (for details, see the SI).

To discover reasonable EC testing conditions for the flexible NPL in two-electrode symmetric devices, different potential windows (Figure S4) and compositions of solid electrolytes (Table S1 and Figures S5–S9) were screened (for details, see the SI). The optimum solid electrolyte composition for the NPL was found to be KOH in poly(vinyl alcohol) (PVA, molecular weight of ~50 000) with weight ratio ~1:1. The operating potential windows were set within −0.8 to 0.8 V (narrow potential window, NPW) and −1.4 to 1.4 V (wide potential window, WPW).

For testing in a NPW, a NPL can only behave as an EDLC by electrostatic adsorption in the 3-D nanoporous structure. However, operating in a WPW, the window is sufficient to trigger an electrochemical conversion from NiF_2 to $Ni(OH)_2$ at ~1–1.2 V, depending on the scan rate. It is interesting that the NPL shows a typical EDLC behavior that is a quasi-rectangular shape in the cyclic voltammograms (CVs) even at high scan rates of 100 V s^{-1} (Figures 2a and S10a). The data establish that the nanoporous structure of the NPL is responsible for the electrostatic adsorption effect during testing and the high electric conductivity of the devices mitigates the polarization effect during CV testing, even at high scan rates up to 100 V s^{-1}. By fitting a log(anodic peak current)–log(scan rate) plot (Figure 2b), a b-value of 0.85 was obtained, which indicates that a surface-controlled electrode process (for capacitive, b = 1) dominates in the device (see the SI). The quasi-triangle shape in galvanostatic discharge/charge (GDC) curves (Figures 2c and S10b) also indicates the EDLC behavior of the NPL. The C_A/C_V (based on the size of the NPL) calculated from CVs (Figure S10c) can reach up to 0.5 mF cm^{-2} (5.6 F cm^{-3} or 2.7 F g^{-1}) at a scan rate of 50 mV s^{-1}, whereas C_A/C_V calculated from the GDC curve (Figure 2c) is 0.29 mF cm^{-2} (3.2 F cm^{-3} or 1.57 F g^{-1}) at 0.1 mA cm^{-2} (0.54 A g^{-1}). To convert NiF_2 to $Ni(OH)_2$, an activation process is initiated by cyclic voltammetry within a WPW (see the SI and Figure S11). It is clear from the CVs (Figures 2d and S12a,b) that a pair of redox peaks at anodic (0.19 V) and cathodic (−0.19 V) sweeps appears after activation. The widening potential difference (ΔV) between the anodic and cathodic peaks with increased scan rates indicates that a diffusion-controlled process dominates the electrode reactions. b = 0.64, obtained after fitting (Figure 2e), also indicates that a diffusion-controlled process (b = 0.5) dominates the electrode reactions. Furthermore, a pair of battery-like plateaus at 0.2/−0.2 V were found from GDC curves (Figures 2f and S12c), which originated from anion (OH^-) intercalation and the reversible reactions between Ni(II) and Ni(III), $Ni(OH)_2 + OH^- \leftrightarrows NiOOH + H_2O + e^-$. The energy storage mechanism of the fabricated devices is similar to that of a Ni–Cd battery.[18] The C_A/C_V calculated from the CVs (Figure S12d) and GDC curves are 75 mF cm^{-2} (833 F cm^{-3} or 407 F g^{-1}) at scan rate of 50 mV s^{-1} and 66 mF cm^{-2} (733 F cm^{-3} or 358 F g^{-1}) at 1 mA cm^{-2} (5.4 A g^{-1}, Figure 2f), which is significantly higher than

dx.doi.org/10.1021/ja501247f | J. Am. Chem. Soc. 2014, 136, 6187–6190

those found in flexible electrodes made with carbonaceous materials such as graphene/polyaniline composite (135 F cm^{-3} at 2 mV s^{-1}),[19] CNTs (less than 16 F cm^{-3} at 1 mV s^{-1}),[20] and carbide-derived carbon materials (up to 90 F cm^{-3} at 1 mA cm^{-2}).[21]

Furthermore, electrochemical impedance spectroscopy (EIS) was used to investigate the kinetic processes of the electrode reactions in the flexible devices. Nyquist plots (Figure 3a) for

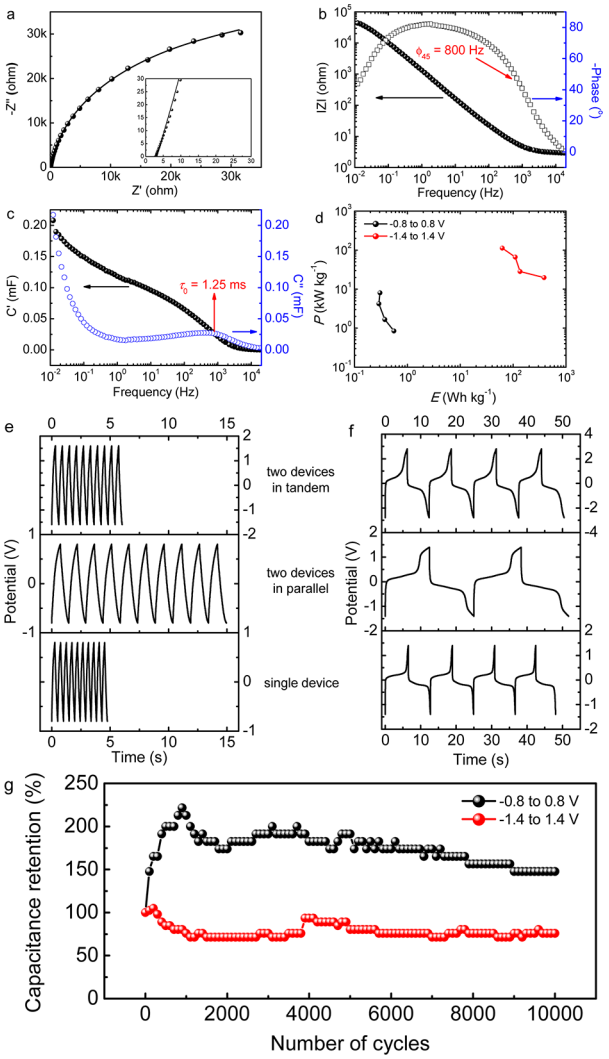

Figure 3. EC performance of the NPL. (a) Nyquist plot of the device tested at the open-circuit potential within the frequency range from 10^{-2} to 10^{4} Hz. The inset shows the enlarged plot in the high-frequency region. (b) Bode plot. (c) Real (C') and imaginary (C'') portions of complex capacitance. (d) Ragone plot. (e,f) GDC curves of a single device and two devices connected in series and in parallel, tested in NPW and WPW, respectively. (g) 10 000 cycle GDC testing within both a NPW (black) and a WPW (red).

the NPL measured at the open-circuit potential (OCP) illustrate an equivalent series resistance (ESR, the intersection with the real axis) of ∼2.8 Ω, which indicates a high ionic conductivity of the solid electrolyte and low interface resistance between the NPL and solid electrolyte. The capacitance response frequency for the flexible device at a phase angle of −45° (ϕ_{45}) was found to be 800 Hz from the Bode plot (Figure 3b), which is equivalent to a relaxation time constant (τ_0) of ∼1.25 ms. This indicates that pseudocapacitive behavior and stored energy are accessible at frequencies below 800 Hz. At 2 Hz, the phase angle for the device is ∼ −82°, which is close to ideal capacitive behavior (−90°). Moreover, τ_0 calculated from the plot of frequency-dependent imaginary capacitance (C'') is consistent with that calculated from the Bode plot, i.e., 1.25 ms (Figure 3c). It is appealing that the value $\tau_0 \approx 1.25$ ms obtained in this work is much lower than those found in most recently published reports, for example, graphene (33 ms),[4] carbon-onions (26 ms),[3] and MnO_x/Au multilayers (4.7 ms).[22] For comparison, the Ragone plot (Figure 3d) was plotted in power density (P) vs energy density (E) for the NPL tested in both the NPW (−0.8 to 0.8 V) and WPW (−1.4 to 1.4 V). The maximum P and E tested in the NPW are 8 kW kg^{-1} and 0.6 Wh kg^{-1}, respectively. The values increase to 112 kW kg^{-1} and 384 Wh kg^{-1}, respectively, when being tested in a WPW. Compared to flexible EC devices based on EDLCs such as CNTs,[23] the NPL delivers better specific power and energy density in the NPW, whereas the NPL shows much higher power supply performance in WPWs than that of pseudocapacitors recently published[24] (for detailed EC performance comparison with some state-of-the-art thin-film or flexible supercapacitors, see Table S2). From a practical view, the EC performance of a flexible device is better measured when it is connected both in tandem and in parallel. It is clear that doubled operation potential windows and GDC durations are obtained from the devices tested within both NPW (Figure 3e) and WPW (Figure 3f) in tandem and in parallel connections, respectively. To characterize the cyclability of the devices, 10 000 GDC cycles (Figure 3g) were performed within both a NPW (at 1 mA cm^{-2} or 5.4 A g^{-1}) and a WPW (at 2 mA cm^{-2} or 10.8 A g^{-1}). It is interesting that the capacitance increased to 220% during the initial 900 cycles in a NPW, which probably indicates a gradual increase in electrochemically active surface area or surface passivation. After 900 cycles, the capacitance gradually decreased and finally stabilized at 150% after 10 000 cycles, which is still higher than the initial capacitance. Similarly, when being tested within the WPW, the devices increased to 105% for the initial 300 cycles and then decreased and stabilized at 76% retention after 10 000 cycles. This indicates that the delivered capacitance based on both EDLCs (NPW) and faradaic reactions (WPW) can maintain over 75% of the initial value over long-term testing, which is promising for practical applications. A more important feature is that, after 10 000 cycles of testing, the NPL still maintained its nanoporous structure (Figure S13), and no decay of the layer was observed. Moreover, after cyclability testing, the ESR increased to only 3.8 Ω (Figure S14), which indicates that the EC testing did not significantly change the solid electrolyte/NPL interface.

The effect of bending on the EC performance was also measured on the NPL-based devices (Figure 4a,b). The delivered capacitance is influenced by the bending angles in a nonlinear fashion (Figures 4c and S15). At bending angles of 90° and 120°, the capacitance increased to 125% and 117%, while the capacitance retention was 80% at the 180° bending angle. In addition, flexibility tests were carried out by bending a device to 180°, 1000 times. The capacitance (Figure 4d) showed a quick drop after the initial few bending cycles, and it was then maintained at 76% capacitance retention. Finally, complementary NPLs based on Fe and Co were prepared using the same fabrication technique (Figure S16). This underscores the generality of the anodization approach.

In summary, a 3-D nanoporous NiF_2-dominant thin-film grown on PET shows good flexibility and can even be

dx.doi.org/10.1021/ja501247f | J. Am. Chem. Soc. 2014, 136, 6187−6190

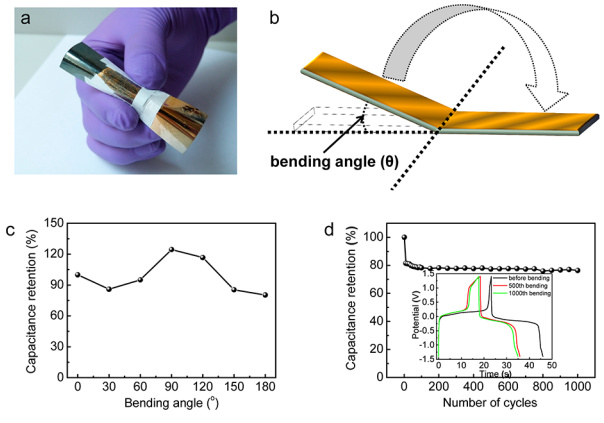

Figure 4. Flexibility tests on the NPL-based EC devices. (a) Photograph of the flexible EC device while bent. (b) Schematic representation of the definition of bending angle. (c) Dependence of capacitance retention on bending angle. (d) Dependence of capacitance retention on bending cycles to 180° bending angle. The inset shows GDC curves recorded before and after bending for 500 and 1000 cycles.

freestanding. The thin-film NPL delivers exacting supercapacitive performance, with a maximum capacitance of 0.29 mF cm^{-2} (3.2 F cm^{-3} or 1.57 F g^{-1}), energy density of 0.6 Wh kg^{-1}, and power density of 8 kW kg^{-1} from electrostatic adsorption, and a maximum capacitance of 66 mF cm^{-2} (733 F cm^{-3} or 358 F g^{-1}), energy density of 384 Wh kg^{-1}, and power density of 112 kW kg^{-1} from faradaic reactions. Flexibility and cyclability tests show that the nanoporous layer maintains its high performance, which is an important advance in flexible devices. The designed approach has the potential of being applied to the fabrication of other metal NPLs.

■ ASSOCIATED CONTENT

Supporting Information

Experimental details and supporting data. This material is available free of charge via the Internet at http://pubs.acs.org.

■ AUTHOR INFORMATION

Corresponding Author

tour@rice.edu

Author Contributions

⊥Y.Y. and G.R. contributed equally to this work.

Notes

The authors declare no competing financial interest.

■ ACKNOWLEDGMENTS

We thank the Peter M. and Ruth L. Nicholas Post-Doctoral Fellowship of the Smalley Institute for Nanoscale Science and Technology for the financial support of Dr. Y. Yang. Further support came from the AFOSR MURI program (FA9550-12-1-0035).

■ REFERENCES

(1) Nyholm, L.; Nyström, G.; Mihranyan, A.; Strømme, M. *Adv. Mater.* **2011**, *23*, 3751.
(2) Jiang, J.; Li, Y.; Liu, J.; Huang, X.; Yuan, C.; Lou, X. *Adv. Mater.* **2012**, *24*, 5166.
(3) Pech, D.; Brunet, M.; Durou, H.; Huang, P.; Mochalin, V.; Gogotsi, Y.; Taberna, P.-L.; Simon, P. *Nat. Nanotechnol.* **2010**, *5*, 651.
(4) El-Kady, M. F.; Strong, V.; Dubin, S.; Kaner, R. B. *Science* **2012**, *335*, 1326.
(5) Yoshino, A. *Angew. Chem., Int. Ed.* **2012**, *51*, 5798.
(6) Horng, Y.-Y.; Lu, Y.-C.; Hsu, Y.-K.; Chen, C.-C.; Chen, L.-C.; Chen, K.-H. *J. Power Sources* **2010**, *195*, 4418.
(7) Meng, C.; Liu, C.; Chen, L.; Hu, C.; Fan, S. *Nano Lett.* **2010**, *10*, 4025.
(8) Kaempgen, M.; Chan, C. K.; Ma, J.; Cui, Y.; Gruner, G. *Nano Lett.* **2009**, *9*, 1872.
(9) Lu, X.; Zhai, T.; Zhang, X.; Shen, Y.; Yuan, L.; Hu, B.; Gong, L.; Chen, J.; Gao, Y.; Zhou, J.; Tong, Y.; Wang, Z. L. *Adv. Mater.* **2012**, *24*, 938.
(10) Wang, G.; Zhang, L.; Zhang, J. *Chem. Soc. Rev.* **2012**, *41*, 797.
(11) Choi, D.; Blomgren, G. E.; Kumta, P. N. *Adv. Mater.* **2006**, *18*, 1178.
(12) Zhang, H.; Zhou, Y.-N.; Sun, Q.; Fu, Z.-W. *Solid State Sci.* **2008**, *10*, 1166.
(13) Lang, X.; Hirata, A.; Fujita, T.; Chen, M. *Nat. Nanotechnol.* **2011**, *6*, 232.
(14) Huang, J.; Sumpter, B. G.; Meunier, V. *Angew. Chem., Int. Ed.* **2008**, *47*, 520.
(15) Wang, H.; Casalongue, H. S.; Liang, Y.; Dai, H. *J. Am. Chem. Soc.* **2010**, *132*, 7472.
(16) Schaedler, T. A.; Jacobsen, A. J.; Carter, W. B. *Science* **2013**, *341*, 1181.
(17) Shi, H.; Lederman, D.; O'Donovan, K. V.; Borchers, J. A. *Phys. Rev. B* **2004**, *69*, 214416.
(18) Casas-Cabanas, M.; Canales-Vazquez, J.; Rodriguez-Carvajal, J.; Palacin, M. R. *J. Am. Chem. Soc.* **2007**, *129*, 5840.
(19) Wang, D. W.; Li, F.; Zhao, J.; Ren, W.; Chen, Z. G.; Tan, J.; Wu, Z. S.; Gentle, I.; Lu, G. Q.; Cheng, H. M. *ACS Nano* **2009**, *3*, 1745.
(20) Futaba, D. N.; Hata, K.; Yamada, T.; Hiraoka, T.; Hayamizu, Y.; Kakudate, Y.; Tanaike, O.; Hatori, H.; Yumura, M.; Iijima, S. *Nat. Mater.* **2006**, *5*, 987.
(21) Fernandez, J. A.; Arulepp, M.; Leis, J.; Stoeckli, F.; Centeno, T. A. *Electrochim. Acta* **2008**, *53*, 7111.
(22) Si, W.; Yan, C.; Chen, Y.; Oswald, S.; Han, L.; Schmidt, O. G. *Energy Environ. Sci.* **2013**, *6*, 3218−3223.
(23) Hyder, M. N.; Lee, S. W.; Cebeci, F. C.; Schmidt, D. J.; Horn, Y. S.; Hammond, P. T. *ACS Nano* **2011**, *5*, 8552.
(24) Wu, C.; Lu, X.; Peng, L.; Xu, K.; Peng, X.; Huang, J.; Yu, G.; Xie, Y. *Nat. Commun.* **2013**, *4*, 2431.